Amphibious robot with self-rotating paddle-wheel mechanism

Chaewon Kim[1], Kyungwook Lee[1], Sijun Ryu[1] and TaeWon Seo[1,*], *Senior Member, IEEE,*

Abstract—Marine transportation is an important means of transportation, in which ships are in constant use and accidents are unavoidable. In this study, we developed an amphibious robot to help rescue people in an accident environment that are too low or dangerous for rescuers to enter. Angled spoke paddling wheel(ASPW) makes it possible to drive on the water surface, while taking advantage of the Angled Spoke Wheel(ASW). The ASPW changes the paddle force by rotating the paddle when the wheel rotates so that the total force is generated in the direction of the robot's movement. The paddle is optimized using the Taguchi method. The driving experiment was conducted in four environments: ground, water surface, transition between ground and water, and obstacle overcoming situation. The maximum driving speed was 0.47 m/s on the ground and 0.1 m/s on the water surface. The maximum average inclination degree in the transition situation was 25° from the ground to the water surface and 20° from the water surface to the ground. Additionally, it was possible to overcome an obstacle with a maximum height of 41.3 mm, demonstrating that the proposed robot excels in amphibious driving, while possessing the ability to overcome the ASW level obstacle.

Index Terms—Amphibious, mobile robot, field robot, angled spoke wheel, obstacle overcoming.

I. INTRODUCTION

HISTORICALLY, the maritime industry has contributed significantly to a country's economic development [1]. With the development of the marine industry, a large amount of marine resources, such as oil and natural gas, and biological resources, such as fish, can be obtained. Additionally, as maritime trade became possible owing to the development of shipbuilding and navigation technologies, economic exchanges with other continents are possible through sea routes, and the economy has developed significantly. In modern times, air transportation has become possible with the development of airplanes, but the demand for maritime trade continues to increase [2].

Accordingly, marine accidents are also increasing. Additionally, the cause of the accident may be the ship's engineering

[1]The authors are with the Department of Mechanical Convergence Engineering, Hanyang University, Seoul 04763, Republic of Korea. (Chaewon Kim, Kyungwook Lee, Sijun Ryu)

[1,*]TaeWon Seo is with the Department of Mechanical Convergence Engineering, Hanyang University, Seoul 04763, Republic of Korea. `corresponding author, phone: +82-2-2220-0428, +82-2-2220-2299, e-mail: taewonseo@hanyang.ac.kr`
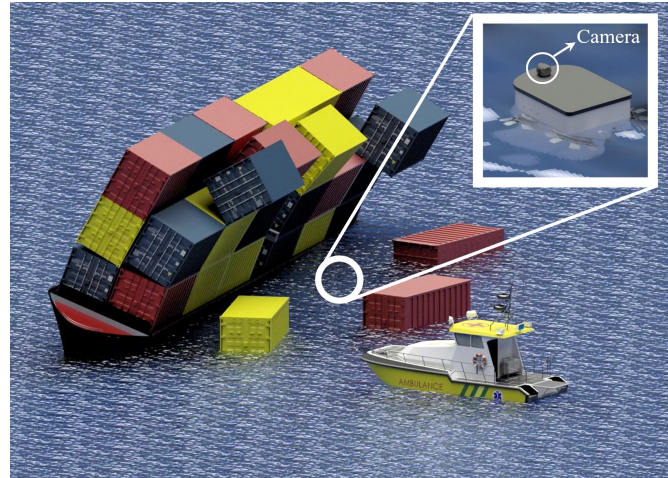
Fig. 1. A situation where a robot enters and explores between narrow structures instead of a rescuer at a disaster rescue site.

problem; however, the International Maritime Organization (IMO) might report that it is a human error and organizational problem [3]. This implies that no matter how advanced shipbuilding and navigation technologies may be in the future, accidents will continue to occur.

When rescuers are sent to the scene for recovery, their lives can be endangered because of the baggage or structures of a ship that are likely to fall. Furthermore, rescue boats may not be able to enter the disaster site due to fallen cargo or structures. This situation is described in Fig. 1. Thus, to understand the specific internal situation and find the victim at the scene of the accident where it is difficult for rescuers to enter, it is better if a robot with cameras or sensors, instead of a person, enters a dangerous site.

Various amphibious robots have been previously studied [4]. Fig. 2 demonstrates the characteristics these amphibious robot. Types of amphibious robots can be largely classified into five types: leg, wheel, paddle, propeller, and bio-inspired. An ALUV [5] is a six-legged robot. The ALUV is small, but it is not suitable for marine rescue because it walks in water slower than robots that are moved by wheels. Wheel-type robots include SeaDog [6], AmphiHex-I [7], AmphiHex-II [8], and Claw-wheel [9]. These robots operate at a high speed on the water surface. Furthermore, they possess good obstacle overcoming ability. However, this type of robot can interfere with the use of cameras and sensors for rescue, as the wheel rotates and the upper parts of the wheel are exposed above the water surface. The eccentric paddle(ePaddle) is
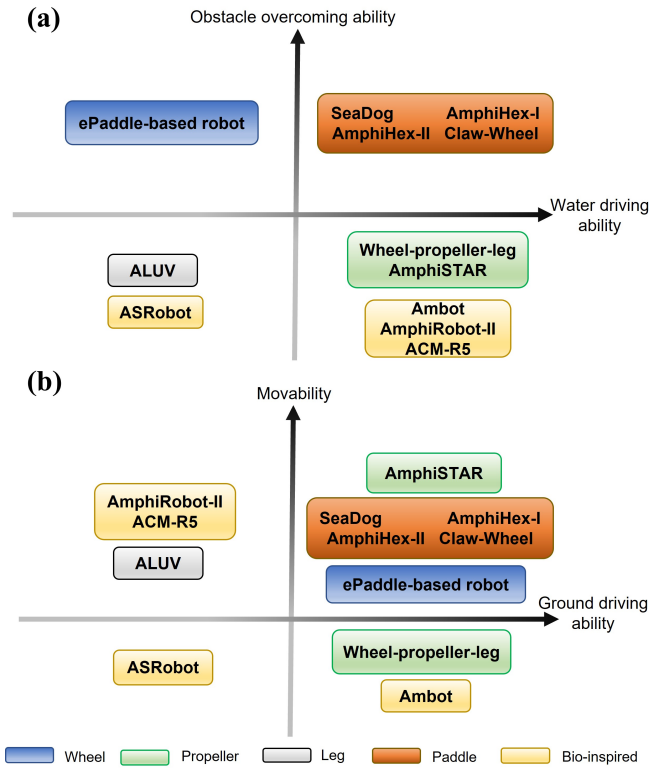
(a)

(b)

Fig. 2. Characteristics of existing amphibious robots. The color of the box indicates the robot's mechanism type. (a) is a graph comparing the performance of obstacle overcoming ability and water driving ability. (b) is a graph comparing the performance of movability and ground driving ability. In (a), quadrant 1 shows high water driving ability and high obstacle overcoming ability, quadrant 2 shows low water driving ability and high obstacle overcoming ability, quadrant 3 shows low water driving ability and low obstacle overcoming ability, quadrant 4 shows high water driving ability and low obstacle overcoming ability. (b) has the same meaning as (a).

a paddle-type amphibious robot. Additionally, they have the disadvantage of exposing the upper parts of the wheels to the water surface [10]. Wheel-propeller legs [11] and AmphiSTAR [12] have high speeds on the water surface because of the propeller. However, these types of robots exhibit poor performance in obstacle-overcoming situations. Bio-inspired robots include AmphiRobot-II [13], ACM-R5 [14], ASRobot [15], and Ambot [16]. However, AmphiRobot-II has difficulty overcoming obstacles on the ground, while ACM-R5 demonstrates extremely slow speed on the ground. Although Ambot performs well on the ground as well as on the water surface, it has a wheel trajectory interference problem, and the robot is not suitable for rescue in water because it cannot enter narrow structures in marine disaster situations.

The reasons why aforementioned amphibious robots listed above are not suitable for marine rescue demonstrate the conditions that marine rescue robots encounter: 1) It must be possible for the marine rescue robot to drive on the surface of water and ground simultaneously. 2) The obstacles must be overcome. 3) The wheel trajectory should not rise to the water surface.

In this study, an amphibious robot applied with an ASPW can compensate for the disadvantages of existing amphibious robots by satisfying these four conditions. An ASPW can pass
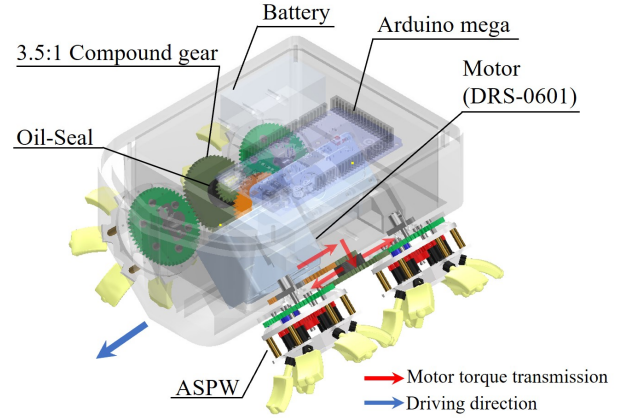

Fig. 3. 3D model of the robot and it's configuration. The red arrow is the transmission path of the motor torque, and the blue arrow is the moving direction of the robot.

through a narrow space by preventing the trajectory of the wheel from rising to the water surface using external and planetary gears, and has the advantages of ASW, fast speed, and ability to overcome obstacles. We optimized the shape of the paddle to be used in the proposed mechanism through an orthogonal array of the Taguchi method to maximize the driving performance.

The remainder of this paper is organized as follows. Section 2 describes the configuration of the robot. Section 3 describes the configuration of the ASPW and analyzes the mechanism. In Section 4, we describe the experiments conducted and analyze the results. Finally, Section 5 presents the conclusions of this study.

II. DESIGN OF THE ROBOT

A. Overall configuration

The overall configuration of the robot is illustrated in Fig. 3. The robot body is designed in the shape of a bow to reduce the water resistance when driving on water. The entire size of the robot is 140 mm × 200 mm × 103 mm, with ASPW and 220 mm × 200 mm × 126 mm without ASPW. The dimension without ASPW is the size of the area exposed to water when the robot enters water. The robot comprises four ASPWs, two motors, batteries, an Arduino board and weighs 1.76 kg. The robot body is 3D printed.

In this study, a Herkulex DRS-0601 motor was used. The robot requires high RPM because it needs to drive quickly. Therefore, a compound gear with a gear ratio of 3.5:1 was used to achieve a sufficient speed. Consequently, when the motor rotates, power is transferred to the compound gear and converted to a sufficiently high RPM. The lower-torque/higher-RPM is transmitted to the ASPW.

B. ASPW

The purpose of the ASPW mechanism is to make water surface driving possible while maintaining the advantages of ASW, such as high speed and ability to overcome obstacles. To achieve this purpose, the spokes should be replaced with
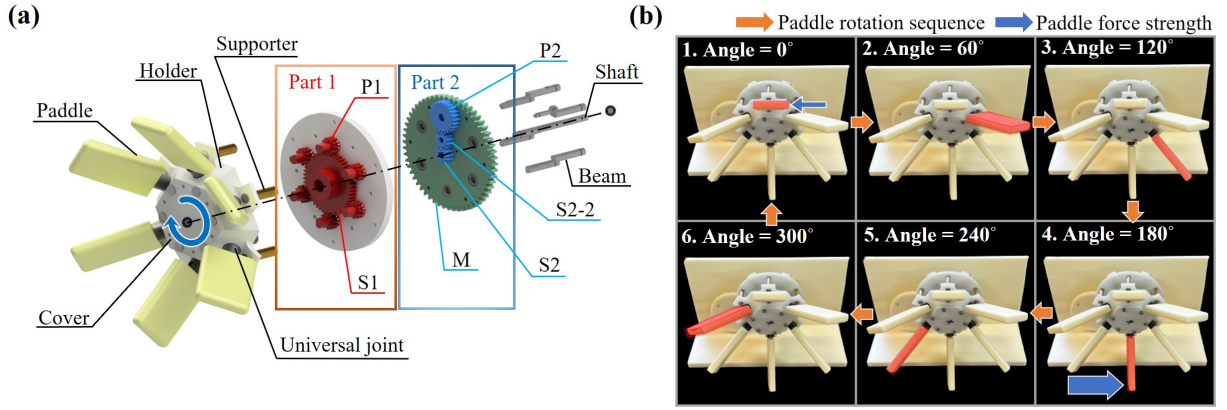
Fig. 4. (a) ASPW configuration. (b) Rotating motion of ASPW. The blue arrows indicate paddle force. The robot movement direction is to the left when the ASPW rotates clockwise.

paddles, and the rotation trajectory of the paddles should not invade the upper part of the robot body like ASW. Then, since the ASPW is completely submerged in water during water surface driving, in order for the robot to move forward, the ASPW's paddle must rotate itself and the force generated by the paddle for each rotation phase must be different. Otherwise, the force generated in the direction of robot movement and the opposite direction to the robot movement are same, so the robot cannot move forward. A design for making an ASPW that satisfies these conditions is described in this section.

1) Configuration: The structure of the ASPW is shown in Fig. 4(a). All shafts and gears are made of stainless steel to prevent rust, and brass bar is used as the support. The remaining components are 3D printed. The ASPW comprises six paddles and a two-part gear set. The paddle was 3D printed with a filament made of Acrylonitiles Styrene Acrylate (ASA). ASA has a sufficient tensile modulus, tensile strength, tensile elongation, flexural modulus, and flexural strength as a rigid body. Therefore the paddle does not deform. In addition, the number of paddles was determined to be six to maintain the balance of the robot well by supporting three points on the ground and to prevents too much stress is concentrated on one spoke. Part 1 consists of planetary gears. Six planetary gears, P1, orbit around sun gear, S1, at the center. Part 2 constitutes three external gears. Gear M rotates the ASPW by receiving power from the motor. The universal joint is connected to P1 gear in part 1 so that the paddle can rotate together as much as P1 rotates. The holder fixes the universal joint, while the cover fixes the six holders.

2) Mechanism: The main shaft in the middle is fixed without rotation. When M receives power from the motor, all parts of the ASPW rotate together because they are constrained by the beams and supports. Because external gears S2, S2-2, and P2 of part 2 have a gear ratio of 1:1:2, when S2 and S2-2 rotate once, P2 rotates half the time. This makes the top paddle and bottom paddle perpendicular to each other when the paddle rotates. Planetary gears S1 and P1 of part 1 determine the angle the paddles form with each other and rotate constantly. The number of gear teeth in S1 is 48 and that in P1 is 12. By designing the number of gear teeth to be

a multiple of six, P1 can be maintained at a constant distance from each other when rotating. S1 and P1 also allow the paddle to rotate at a constant angle of 30° with each other when rotating.

Consequently, the ASPW moves, as shown in Fig. 4(b). Since all paddles have the same cycle, one paddle cycle dyed in red is representatively described. When the paddle is on top(1. Angle = 0°), the paddle force opposite the robot's direction of movement is minimal. However, after rotating 180°(4. Angle = 180°), the maximum paddle force is generated, which has the same movement direction as the robot. This is because the gears of the ASPW rotate and revolve around the paddle, and the area in contact with water changes regularly. The force produced by the paddle can be expressed as (1) [17].

$$F = (C_D + C_L)\frac{rv^2A}{2}[N]. \qquad (1)$$

F is the paddle force, C_D is the drag coefficient, C_L is the lift coefficient, r is the distance between the centroid of the paddle and the axis of rotation, v is the water velocity, and A is the orthogonal projection area where the paddle is in water. Assuming that the paddle shape and experimental environment are the same, F varies according to A. Thus, when the ASPW rotates, the paddle is also self-rotating, so A of the paddle changes. Thus, F also changes. When the paddle on top(1. Angle = 0°), as shown in Fig. 4(b), A is minimum, so F is also minimum. Similarly, when the paddle is at the bottom(4. Angle = 180°), as shown in Fig. 4(b), A is maximum, so F is also maximum.

3) Gear transmission analysis: The ASPW comprises many gears. The power transmission between gears must be conducted effectively so that strong power is transmitted to the paddle without losing as much power as possible. To facilitate water driving by generating a stable paddle force through tight geometrical constraints, ASPW gears were designed considering the results obtained by performing gear transmission analysis [18]. The analysis is as follows.

In part 1, let's say P1 is gear A and S1 is gear B. Gear A and B mesh externally, the speed of contact point v is

$$v = r_A\omega_A = r_B\omega_B \in \mathbb{R}, \qquad (2)$$

TABLE I
DESIGN PARAMETER COMBINATIONS BY ORTHOGONAL ARRAY $\mathbf{L}_9(3^4)$ AND EXPERIMENT RESULTS.

Experiment number	Design parameter				User condition									S/N ratio (dB)
	A	B	C	D	E (gf)									
	Level				Level 1			Level 2			Level 3			
1	1	1	1	1	16.75	15.64	15.55	34.37	33.99	33.61	54.74	53.84	54.55	27.67
2	1	2	2	2	10.86	11.08	10.15	21.79	23.27	22.88	55.86	53.74	53.33	24.33
3	1	3	3	3	11.44	12.49	11.1	34.77	31.49	32.49	68.37	66.39	64.88	25.46
4	2	1	2	3	8.84	8.69	8.61	17.01	14.87	15.99	22.85	21.67	20.67	21.92
5	2	2	3	1	11.45	10.28	10.86	20.74	21.3	21.08	51.14	48.68	49.73	24.28
6	2	3	1	2	11.21	10.8	10.49	23.22	22.5	21.79	24.64	20.74	23.35	23.82
7	3	1	3	2	2.26	2.28	2.36	3.62	2.95	2.63	0	0	0	9.98
8	3	2	1	3	1.88	1.3	1.62	0.73	0.85	0.77	0.2	0	0	-5.52
9	3	3	2	1	2.2	1.36	1.64	0.73	0.89	0.75	0.07	0.05	0.09	-18.85
Optimal	1	1	3	1	15.12	16.73	16.15	39.28	39.38	35.98	64.74	64.46	64.43	27.91

$$\zeta = \frac{\omega_A}{\omega_B} = \frac{r_B}{r_A} < 1. \qquad (3)$$

And if gear A's pitch circle called r_A, root circle called r'_A, outside circle called r''_A, The order of diameter sizes is as follows $r''_A > r_A > r'_A$. Likewise gear B's order of diameter size is as follows $r''_B > r_B > r'_B$. If the radius of the shaft is r_1 and the radius of the beam is r_2, then the relationship between d_0 and r_1 and r_2 is

$$d_0 > r_1 + r_2. \qquad (4)$$

The center distance of two gears A and B is

$$d_0 = r_A + r_B. \qquad (5)$$

Express ζ differently using (3) and (5)

$$\zeta = \frac{r_B}{r_A} = \frac{d_0 - r_A}{r_A} = \frac{d_0}{r_A} - 1. \qquad (6)$$

To summarize the geometric constraints for the tight meshes of gears A and B,

$$\begin{cases} \zeta = \dfrac{r_B}{r_A} = \dfrac{d_0 - r_A}{r_A} = \dfrac{d_0}{r_A} - 1, \\ d_0 = r_A + r_B, \\ r''_A + r_2 - d_0 > r_A > r'_A - r_1, \\ r''_B + r_1 - d_0 > r_B > r'_B - r_2. \end{cases} \qquad (7)$$

Next, we obtain the feasible range of ζ by (7),

$$\frac{d_0}{r''_A + r_2 - d_0} - 1 < \zeta < \frac{d_0}{r'_A - r_1} - 1. \qquad (8)$$

If r_A and r_B are obtained using (5) and (6),

$$r_A = \frac{d_0}{\zeta + 1}, \quad r_B = d_0 - \frac{d_0}{\zeta + 1}. \qquad (9)$$

The same process can be applied to gears S2, S2-2, and P2 of Part 2.

Applying the above analysis and determining r_A(P1) and r_B(S1) in Part 1, when the distance d_0 between the shaft and the beam is set to 15 mm, r_A is 3 mm, r_B is 12 mm. Similarly, in the case of r_A of S2 and r_B of S2-2, r_A is 3 mm and r_B is 3 mm. Finally, in the case of r_A of S2-2 and r_B of P2, r_A is 3 mm and r_B is 6 mm. The ASPW is designed based on the geometric constraints obtained from the analysis above.

III. ASPW PADDLE DESIGN

The drag coefficient C_D depends on the paddle shape, which implies that depending on the design of the paddle, the robot's driving speed on the water surface can be increased or decreased.

Previous underwater propulsion optimization studies have often optimized designs through computer simulations or analytical programs (particularly propellers) [19]–[21]. However, it is difficult to numerically predict or simulate the ASPW. This is because the ASPW does not always generate constant forces such as a normal propeller. ASPW is a mechanism that did not exist before, it was not possible to specifically predict which input would affect which output. And since ASPW was not a very complex system, it was judged that simulation using high-performance software was not cost-effective.

Therefore, in this study, the Taguchi method was used to experimentally obtain the optimal design value for the paddle shape of the ASPW. The Taguchi method is an experimental design method that optimizes the design by considering unpredictable external factors during the design stage. Therefore, it is suitable in situations wherein the analysis is difficult [22], [23]. In fact, the validity of the Taguchi method is proven through cases in which optimized results are obtained using the Taguchi method [24]–[26]. The signal-to-noise (S/N) ratio was set to (10) to obtain the maximum paddle force.

$$S/N ratio = -10log\left|\frac{(\frac{1}{y_1})^2 + (\frac{1}{y_2})^2 + \cdots + (\frac{1}{y_n})^2}{n}\right| [dB]. \quad (10)$$

$y_1 \cdots y_n$ is the paddle force, which is the result of the experiment, and n is the number of experiments performed for each design parameter. A high S/N ratio indicates high sensitivity to that design parameter. This implies that the design parameter combination is closer to the optimal value.

The selected design parameters were the X-axis curvature, Y-axis curvature, pitch angle, and end shape of the paddle. The X- and Y-axis curvatures and pitch angles were selected because they affect the thrust force that closely related to paddle performance according to the changes [27]. The end effect of the paddle was selected because C_D that affects thrust force depends on the projection shape that meets the water [28]. Table I lists the combinations of design parameters and
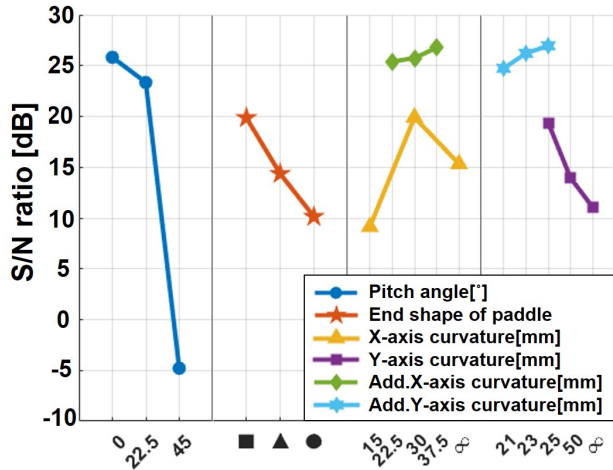
Fig. 5. S/N ratio of each design parameter. Add. means it is additional experiment's result.

Fig. 6. (a) ASPW with finally designed paddles apllied. (b) Design parameters of ASPW.

Fig. 7. Overall test setup comprising a ground part, a water part, and a slope for a transition situation. Slope can change the inclination angle θ. Photo sensors are installed in the ground part and water part at 1-m intervals.

their experimental results by the orthogonal array $\mathbf{L}_9(3^4)$ of the Taguchi method. The selected design parameter levels were as follows: X-axis curvature: ∞ mm, 15, and 30 mm; Y-axis curvature: ∞ mm, 25, and 50 mm; end shape of paddle: ■, ▲, ●; pitch angle: 0°, 22.5°, and 45°, which means levels 1, 2, and 3 in order. The user condition was as follows: motor RPM: 60 RPM, 90 RPM, and 120 RPM which means levels 1, 2, and 3 in order. Experiment number is a list of combinations of each level according to $\mathbf{L}_9(3^4)$. Each experiment was performed 3 times. A means pitch angle, B means end shape of paddle, C means X-axis curvature, D means Y-axis curvature and E means motor RPM. On the far right of the table, the S/N ratio obtained through the experiment and (10) is shown.

Fig. 5 shows the S/N ratio of Table I as a graph. In the first experimental result, the optimal values were pitch angle of 0°, rectangular end shape of the paddle, X-axis curvature of 30.5 mm, and Y-axis curvature of 25 mm. As for the pitch angle, as the paddle rotates, the angle continues to change positively and negatively, so even if an additional experiment is conducted with a negative angle(less than 0°), the S/N ratio graph will come out symmetrically. So 0° was decided as the optimal value. Since the end shape of paddle is not a continuous variable, the optimal shape was determined as a rectangle. However, since the X- and Y-axis curvature may have higher values around the peak value, it was decided to conduct additional experiments.

As a result of all experiment, the optimal paddle design parameters that demonstrated the highest performance were X-axis curvature of 37.5 mm, Y-axis curvature of 25 mm, rectangular end shape of the paddle, and pitch angle of 0°. At 120 RPM the paddle force improved by 18.27% over the basic paddle shape.

The detailed optimization process of the paddle design, such as the reason for using the Taguchi method, which is an experimental optimization technique, the test setup, the reason for selecting design parameters, and the detailed experimental results, is described in [29].

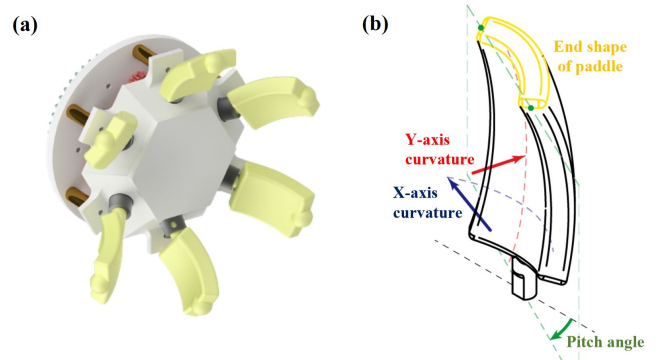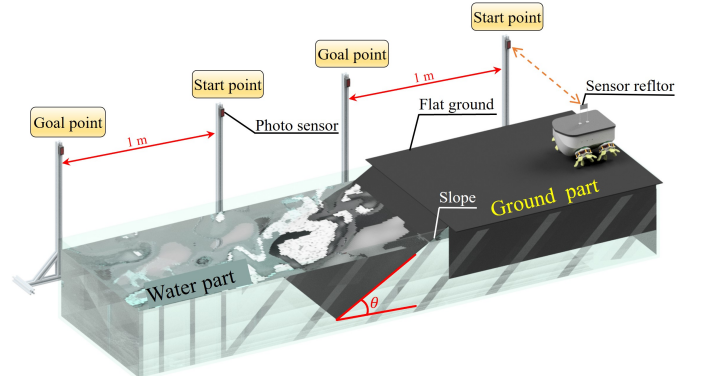The final design with the obtained design parameters is il-

lustrated in Fig. 6(a). The four design parameters of the paddle are illustrated in Fig. 6(b). The paddle was designed with the values obtained using the Taguchi method. A spherical point was added to the bottom of the paddle. Thus, a single contact rather than a line contact was made on the ground, considering the fact that a single contact performs better when driving on the ground in previous studies [30].

IV. EXPERIMENTAL RESULTS AND DISCUSSION

Three experiments were performed to test and prove the performance of the ASPW:1) ground driving ability, 2) comparison of driving ability between the ASPW and conventional paddle wheel, 3) inclination degree that can be overcome in a transition environment, and 4) obstacle overcoming ability.

A. Testbench setup

Fig. 7 demonstrates the overall test setup used in the experiment. For ground and surface driving tests, a photo sensor (PB-R1P) was used to measure the speed of the robot. When the photo sensor at the starting point and the goal point detects the reflector on the robot, it records the time. The sensors were arranged at 1-m intervals of, and the speed was measured by calculation. To test the situation in which the robot transitions from land to water, a slope was installed, and the maximum slope that can be climbed was tested by changing θ. In the case of the obstacle overcoming experiment, a rectangular object
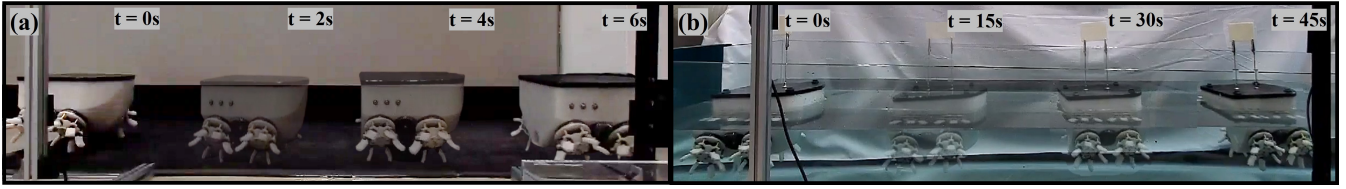
Fig. 8. (a) Ground driving ability experiment. (b) Water surface driving ability experiment. The results of water surface driving experiments of ASPW and conventional paddles were compared on this test bench. Refer to multimedia extension for the experiment.
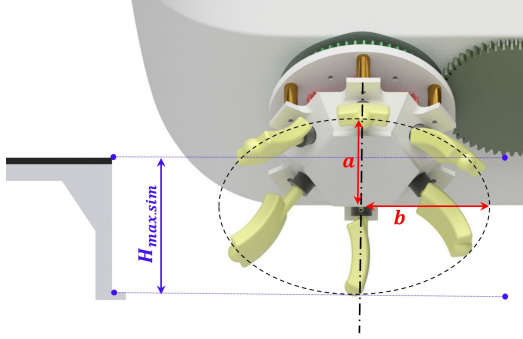

Fig. 9. ASPW trajectory. The short axis of the ellipse is a and the long axis of the ellipse is b. $H_{max.sim}$ is the theoretical maximum height that can overcome obstacles.

was installed on a flat ground and the maximum height was tested.

B. Ground driving ability

The experiment was conducted on the flat ground part shown in Fig. 7 with photo sensor. The test conditions for RPMs were 60 RPM, 90 RPM, 120 RPM, and 135 RPM. Each speed measurement was performed in triplicate. In each experiment, the speed was almost the same. On average, it was 0.19 m/s at 60 RPM, 0.31 m/s at 90 RPM, 0.4 m/s at 120 RPM, and 0.47 m/s at 135 RPM.

As shown in Fig. 9, the major axis a, minor axis b and perimeter L of the ASPW trajectory depend on the paddle length. Therefore, the method of estimating the ground speed of the robot considering the length of the paddle is as follows:

$$v = RPM \left(\frac{L}{rev} \right) \left(\frac{min}{60sec} \right) [m/s]. \tag{11}$$

v is the speed of the robot on the ground, and L is the perimeter of the ASPW trajectory projection. According to ASW's rotational transformation and projection from the spoke trajectory method, the projection of the ASPW trajectory is elliptical [31]. Fig. 9 shows ASPW's trajectory. Therefore, L can be expressed using the following approximate expression:

$$L = 2\pi \sqrt{0.5(a^2 + b^2)} [m]. \tag{12}$$

For ASPW used in this paper, L was 0.21m. By substituting the calculated L value and each driving RPM into (11), it is 0.21 m/s at 60 RPM, 0.32 m/s at 90 RPM, 0.42 m/s at 120 RPM, 0.47 m/s at 135 RPM. Thus it can be confirmed that the experimental results agree with the calculations. Fig. 8(a) describes ground driving test in time order.

C. Comparison of driving ability between ASPW and conventional paddle wheel

The experiment was conducted on the water section shown in Fig. 7 using the same method as the ground driving test, with four RPMs, 60 RPM, 90 RPM, 120 RPM, and 135 RPM, as in the ground driving experiment. Each measurement was performed thrice. For the robot with the ASPW applied, it was 0.025 m/s at 60 RPM, 0.049 m/s at 90 RPM, 0.077 m/s at 120 RPM, and 0.1 m/s at 135 RPM. However, when using the same mechanism as the existing paddle-type amphibious robot without ASPW, the robot could not move forward.

As explained in the ASPW mechanism in Section 2, in the case of an ASPW, the paddle force is controlled by the rotation of the paddle. Therefore, even if the wheel rotates while being completely submerged in water, the force generated in the direction of the robot's travel is stronger than that in the opposite direction. However, if it is not applied with the ASPW, the number 1(1. Angle = 0°) sequence paddle force and the number 4(1. Angle = 180°) paddle force shown in Fig. 4(b) will be the same. Therefore, the robot can not move forward on the water surface. In other words, in the case of a normal paddle, the paddle force in the direction opposite to the movement is generated equally, and thus the resultant force becomes zero. Therefore, the robot wheels rotate but remain stationary regardless of the RPM in the experiment when using the existing mechanism in which the ASPW is not applied. Fig. 8(b) shows the robot driving on the water surface in time order.

D. Inclination degree that can be overcome in transition environment

An amphibious robot may encounter a transition situation from the ground to the water surface or from the water surface to the ground. Therefore, an experiment was conducted to observe how much inclination it can overcome in the transition situation. In this experiment, the maximum a degree of inclination was found while adjusting the θ of the slope of Fig. 7.

Fig. 10(a) shows the behavior of the robot in the ground to water surface transition situation. In this case, driving up to a slope of 25° is possible. A characteristic of the transition situation is that the moment the robot is submerged in water, and buoyancy is generated by the volume of the submerged fluid. When the robot is on the ground, the reaction forces of the front wheel (F_1) and rear wheel (F_2) are the same. However, when the transition occurs, the front wheel enters the water first and the front part of the robot body is submerged
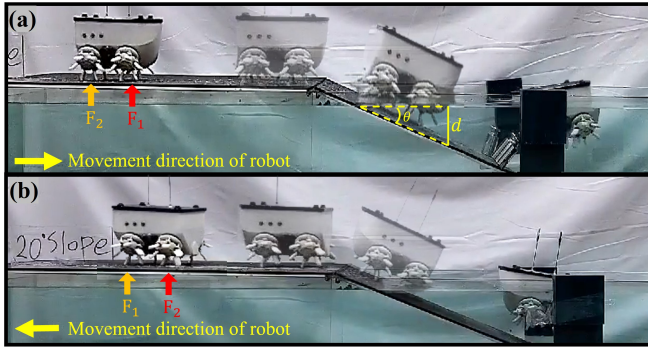
Fig. 10. (a) Ground to water surface transition experiment. (b) Water surface to ground transition experiment. Refer to multimedia extension for the experiment.
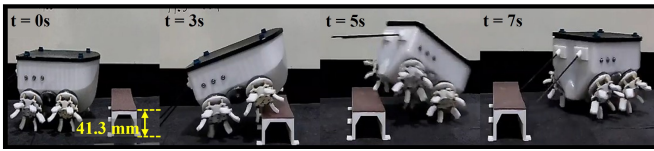

Fig. 11. Obstacle overcoming experiment. Refer to multimedia extension for the experiment.

Fig. 12. Percentage of maximum obstacle overcoming height relative to wheel size of amphibious robots.

in water. Additionally, buoyancy is generated. Therefore, the buoyancy force increase, reducing the total reaction force of the front wheel. As F_2 became greater than F_1, the robot rolls forward. The buoyancy increases as the depth(d) of the front part of the submerged robot increases. If the inclination angle is θ, d can be expressed as $d = l\sin\theta$. In this experiment, the point of θ at which F_1 becomes sufficiently smaller than F_2 to cause the robot to lose its balance appears to be between $25°$ and $30°$.

Fig. 10(b) shows the behavior of the robot in the water surface to ground transition situation. In this case, the transition is possible up to a slope of $20°$. The reason seems to be that, as in the case of the ground to water surface transition, the reduction of F_2 due to buoyancy does not support the ground properly, resulting in slip of the wheel. Here, the limit of θ is $20°$ to $25°$.

E. Obstacle overcoming performance

An experiment was conducted to confirm whether ASPW has the ability to overcome obstacles equivalent to ASW. According to the ASW research referenced in this paper, the height of the first spoke that touches the top of the obstacle determines the obstacle-overcoming height. Therefore, this height depends on the spoke length, and rotational transformation and projection from the spoke trajectory were performed to predict the height [31]. Prior to the experiment, the maximum obstacle height that the ASPW could overcome was predicted by considering the paddle length of the ASPW in this way. As a result, as shown in Fig. 9, $H_{max.sim}$ was 41.8mm. The experiment confirmed that the robot can overcome obstacles that have a height of 41.3 mm. Although there is a slight difference between the numerical calculation and the experimental results in the maximum height of obstacles
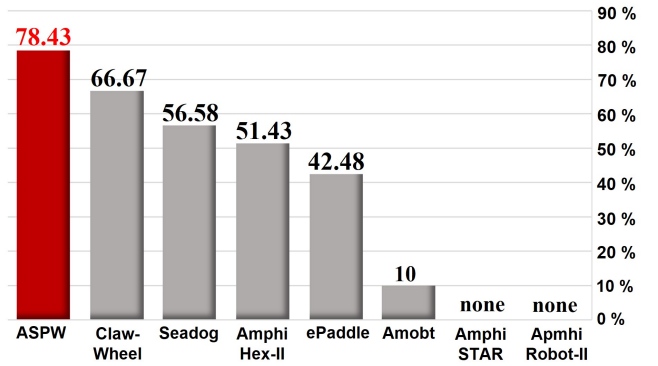
that can be overcome, their values are nearly the same ability to overcome obstacles. Fig. 11 describes the robot overcoming a 41.3 mm high obstacle.

Fig. 12 is a graph comparing the percentage of maximum obstacle overcoming height relative to the wheel size of amphibious robots. Robots that performed obstacle overcoming experiments were compared, and it was assumed that there was no meaningful obstacle overcoming height for robots that only performed rough terrain driving experiments. Through Fig. 12, it is possible to obtain insight that the ASPW has an improved obstacle overcoming ability than the existing amphibious robot's wheel mechanism.

F. Field test

The robot also showed good mobility in various environments. The field test was conducted in a total of 5 environments: grass field, sand field, low space, gravel field, and stream. Fig. 13(a) describes a driving test on a lawn composed of soft soil. It was confirmed that the spokes can be driven even in uneven environments where the spokes are not rigid. Steering was also possible smoothly, so it was easy to look around. Fig. 13(b) describes a driving test conducted on a sandy playground often studded with large stones. It was confirmed that irregularly shaped obstacles of 41.3 mm or less could be overcome. Fig. 13(c) is an image of exploring under a car assuming a situation where it is difficult for people to enter at a disaster site. The camera mounted on the robot made it possible to grasp the situation instead of a person in an area where it is difficult or dangerous for rescuers to enter. Fig. 13(d) represents a driving test conducted on a gravel field. The size of the gravels ranged from 50 to 80 mm in width and 20 to 40 mm in height. Through this experiment, it was confirmed that driving is possible even on very irregular and rough terrain. Fig. 13(e) shows a driving test on a flowing stream. As a result of the experiment, it was confirmed that it was possible to drive in an environment with real water and that it was well waterproofed.

V. CONCLUSION

This study developed an amphibious robot that can drive on a water surface while maintaining the advantages of ASW.
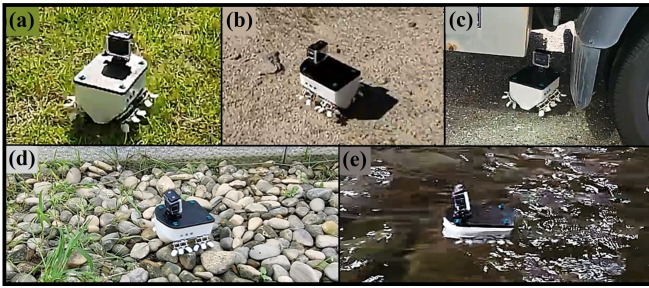
Fig. 13. Field test to demonstrate the robot's driving performance. (a) is Grass field. (b) is sand field with some stones. (c) is low space. (d) is gravel field. (e) is stream. Refer to multimedia extension for the experiment.

Therefore, an ASPW, an amphibious mechanism that did not exist before, is designed to achieve this purpose and create a robot that complements the shortcomings of previous amphibious robots. The paddle design was optimized using the Taguchi method. As a result of the experimental performance of the robot, the robot showed good performance in ground driving, overcoming obstacles, and climbing up in transition environment. The ground driving ability and obstacle overcoming ability depends on the length of the paddle, and the water surface driving ability depends on the area of the paddle, so if the size of the robot and paddle is increased, it will exhibit a faster speed and better ability to overcome obstacles. In the case of uneven terrain such as an outdoor environment, it was observed that the robot could drive well. Although the robot's water surface driving speed is relatively small, future work will try to solve this by increasing the paddle size and designing the robot body to reduce fluid resistance.

REFERENCES

[1] J. Fernández-Macho, P. González, and J. Virto, "An index to assess maritime importance in the european atlantic economy," *Marine Policy*, vol. 64, pp. 72–81, 2016.

[2] D.-W. Song and P. Panayides, *Maritime logistics: A guide to contemporary shipping and port management*. Kogan Page Publishers, 2015.

[3] H.-T. Kim, S. Na, and W.-H. Ha, "A case study of marine accident investigation and analysis with focus on human error," *Journal of the ergonomics society of Korea*, vol. 30, no. 1, pp. 137–150, 2011.

[4] K. Ren and J. Yu, "Research status of bionic amphibious robots: A review," *Ocean Engineering*, vol. 227, p. 108862, 2021.

[5] H. Greiner, A. Shectman, C. Won, R. Elsley, and P. Beith, "Autonomous legged underwater vehicles for near land warfare," in *Proceedings of Symposium on Autonomous Underwater Vehicle Technology*. Ieee, 1996, pp. 41–48.

[6] M. A. Klein, A. S. Boxerbaum, R. D. Quinn, R. Harkins, and R. Vaidyanathan, "Seadog: A rugged mobile robot for surf-zone applications," in *2012 4th IEEE RAS & EMBS International Conference on Biomedical Robotics and Biomechatronics (BioRob)*. IEEE, 2012, pp. 1335–1340.

[7] S. Zhang, Y. Zhou, M. Xu, X. Liang, J. Liu, and J. Yang, "Amphihex-i: locomotory performance in amphibious environments with specially designed transformable flipper legs," *IEEE/ASME Transactions On Mechatronics*, vol. 21, no. 3, pp. 1720–1731, 2015.

[8] B. Zhong, S. Zhang, M. Xu, Y. Zhou, T. Fang, and W. Li, "On a cpg-based hexapod robot: Amphihex-ii with variable stiffness legs," *IEEE/ASME Transactions on Mechatronics*, vol. 23, no. 2, pp. 542–551, 2018.

[9] C.-Y. Huang, C.-N. Kuo, L.-H. Pan, S.-Y. Lin, and J. J. Chou, "Claw-wheel: A transformable robot for search and investigation in amphibious environment," in *2017 IEEE/RSJ International Conference on Intelligent Robots and Systems (IROS)*. IEEE, 2017, pp. 6541–6546.

[10] Y. Sun, S. Ma, K. Fujita, Y. Yang, and H. Pu, "Modeling the rotational paddling of an epaddle-based amphibious robot," in *2012 IEEE/RSJ International Conference on Intelligent Robots and Systems*. IEEE, 2012, pp. 610–615.

[11] J. Yu, Y. Tang, X. Zhang, and C. Liu, "Design of a wheel-propeller-leg integrated amphibious robot, 2010 11th int. conf," *Control, Automation, Robotics and Vision Singapore*, vol. 7.

[12] A. Cohen and D. Zarrouk, "The amphistar high speed amphibious sprawl tuned robot: Design and experiments," in *2020 IEEE/RSJ International Conference on Intelligent Robots and Systems (IROS)*. IEEE, 2020, pp. 6411–6418.

[13] J. Yu, R. Ding, Q. Yang, M. Tan, W. Wang, and J. Zhang, "On a bio-inspired amphibious robot capable of multimodal motion," *IEEE/ASME Transactions On Mechatronics*, vol. 17, no. 5, pp. 847–856, 2011.

[14] H. Yamada, "S. development of amphibious snake-like robot acm-r5," in *the 36th International Symposium on Robotics (ISR 2005), Tokyo*, 2005.

[15] H. Xing, S. Guo, L. Shi, X. Hou, Y. Liu, H. Liu, Y. Hu, D. Xia, and Z. Li, "A novel small-scale turtle-inspired amphibious spherical robot," in *2019 IEEE/RSJ International Conference on Intelligent Robots and Systems (IROS)*. IEEE, 2019, pp. 1702–1707.

[16] L. Cui, P. Cheong, R. Adams, and T. Johnson, "Ambot: A bio-inspired amphibious robot for monitoring the swan-canning estuary system," *Journal of Mechanical Design*, vol. 136, no. 11, 2014.

[17] Y. Liu, "Development and computational validation of an improved analytic performance model of the hydroelectric paddle wheel," *Distributed Generation and Alternative Energy Journal*, vol. 30, no. 1, pp. 58–80, 2015.

[18] B. Luo, W. Cui, and W. Li, "Active and robust twisting morphing wings with geometric constraints for flying or swimming robots," *IEEE/ASME Transactions on Mechatronics*, 2022.

[19] M. Morgut and E. Nobile, "Influence of grid type and turbulence model on the numerical prediction of the flow around marine propellers working in uniform inflow," *Ocean Engineering*, vol. 42, pp. 26–34, 2012.

[20] A. Baquero and A. Haimov, *Marine propeller performance: Computational prediction and experimental validation*. WIT Press, 1999, vol. 22.

[21] J. Sahili and K. Zaidan, "Rov propellers optimization using cad design and cfd modeling and experimental validation," in *2018 6th RSI International Conference on Robotics and Mechatronics (IcRoM)*. IEEE, 2018, pp. 418–421.

[22] K. Yang and B. S. El-Haik, *Design for six sigma: a roadmap for product development*. McGraw-Hill Education, 2009.

[23] R. N. Kacker, E. S. Lagergren, and J. J. Filliben, "Taguchi's orthogonal arrays are classical designs of experiments," *Journal of research of the National Institute of Standards and Technology*, vol. 96, no. 5, p. 577, 1991.

[24] M. Choi, H. Chae, K. Kim, and T. Seo, "Robust design of a rope ascender based on geometric parameters of traction sheave," *International Journal of Precision Engineering and Manufacturing*, vol. 22, no. 5, pp. 965–974, 2021.

[25] Y. Lee, D. Kwon, C. Park, M. Seo, and T. Seo, "Automated technique for high-pressure water-based window cleaning and accompanying parametric study," *Plos one*, vol. 15, no. 12, p. e0242413, 2020.

[26] C. Seo, K. Lee, D. Son, and T. Seo, "Robust design of a screw-based crawling robot on a granular surface," *IEEE Access*, vol. 9, pp. 103 988–103 995, 2021.

[27] D. Sumner, E. Sprigings, J. Bugg, and J. Heseltine, "Fluid forces on kayak paddle blades of different design," *Sports Engineering*, vol. 6, no. 1, pp. 11–19, 2003.

[28] M. Sadraey and D. Müller, "Drag force and drag coefficient," *M. Sadraey, Aircraft Performance Analysis. VDM Verlag Dr. Müller*, 2009.

[29] C. Kim, S. Han, J. Won, and T. Seo, "Empirical optimization of an angled spoke paddling wheel with self-rotating mechanism," *Scientific Reports*, vol. 12, no. 1, p. 20511, Nov 2022.

[30] K. Lee, S. Ryu, C. Kim, and T. Seo, "A compact and agile angled-spoke wheel-based mobile robot for uneven and granular terrains," *IEEE Robotics and Automation Letters*, vol. 7, no. 2, pp. 1620–1626, 2022.

[31] Y. Lee, D. Yoon, J. Oh, H. S. Kim, and T. Seo, "Novel angled spoke-based mobile robot design for agile locomotion with obstacle-overcoming capability," *IEEE/ASME Transactions on Mechatronics*, vol. 25, no. 4, pp. 1980–1989, 2020.